



Trans. Nonferrous Met. Soc. China 33(2023) 3625-3640

Transactions of Nonferrous Metals Society of China

www.tnmsc.cn



# Hot-rolling process and properties of large thickness ratio Al/Mg/Al laminates

Ting LI<sup>1,2,3</sup>, Tao WANG<sup>1,2,3</sup>, Wen-wen LIU<sup>1,2,3</sup>, Zhi-quan HUANG<sup>4</sup>, Zheng-yi JIANG<sup>3</sup>, Qing-xue HUANG<sup>1,2,3</sup>

- 1. College of Mechanical and Vehicle Engineering, Taiyuan University of Technology, Taiyuan 030024, China;
  - 2. Engineering Research Center of Advanced Metal Composites Forming Technology and Equipment, Ministry of Education, Taiyuan 030024, China;
    - 3. TYUT-UOW Joint Research Center, Taiyuan University of Technology, Taiyuan 030024, China;
- 4. School of Mechanical Engineering, Taiyuan University of Science and Technology, Taiyuan 030024, China

Received 10 June 2022; accepted 7 December 2022

Abstract: Large thickness ratio Al/Mg/Al laminates with the initial thickness ratio (ITR, the ratio of initial thickness of a single Mg layer to initial thickness of a single Al layer) ranging from 5 to 40 were prepared by hot rolling. The effects of ITR on the stress and strain fields, microstructure evolution and properties of Al/Mg/Al laminates were investigated by means of simulations and experiments. The results show that with increasing ITR, the ultimate tensile strength and yield strength of the laminates increase, while the interfacial bonding strength and elongation increase first and then decrease, and reach their maximum values of 12.3 N/mm (peel strength) and 23.32%, respectively, when the ITR is 20. At this time, the laminates have the best comprehensive mechanical properties, the deformation coordination ability between component metals is the best, and the texture on the Al side changes to shear texture. After the ITR reaches 40, the bonding performance of the laminates decreases, and the performance of the magnesium alloy is dominant.

Key words: Al/Mg/Al laminates; large thickness ratio; mechanical properties; interfacial bonding strength; microstructure

#### 1 Introduction

Magnesium alloys have the advantages of light weight, high specific strength, high specific rigidity and good electromagnetic shielding property [1–3]. These alloys are widely used in the aerospace, automobile, and electronic product fields [4–6]. However, because of the lack of the corrosion resistance [7–11], their application range is greatly limited. To solve this problem, scholars cladded a layer of aluminum strips with light mass and good corrosion resistance on the surface of magnesium alloy plates to prepare Al/Mg/Al laminates [12–17], which combines the advantages of magnesium alloy and aluminum and has become a material that can

be widely used.

The preparation methods of the Al/Mg/Al laminates mainly include the porthole die co-extrusion process [18,19], lost foam casting liquid–liquid compound process [20], vacuum diffusion bonding [21], friction stir welding [22,23], explosive welding [8,24] and rolling. Compared with other processes, the rolling process has the characteristics of flexible product specifications, stable quality, high production efficiency and ease of large-scale manufacture, and it has gradually become the main method of laminate preparation. In this regard, CHEN et al [25] carried out five-pass rolling of Al/Mg/Al laminates with the Al–Mg–Al initial thickness ratio (ITR, the ratio of initial thickness of a single Mg layer to initial thickness of

a single Al layer) of 1 and found that the threshold bonding reduction ratio in the first pass of Al/Mg/Al laminates at 440 °C was not less than 45%. The Al/Mg/Al laminates (ITR=2) were fabricated by ZHANG et al [26]. It was found that the bonding strength of the laminates and the thickness fraction of the Mg layer after hot rolling decreased with increasing reduction ratio and rolling temperature. WEI et al [27] studied the bonding strength of Al/Mg/Al laminates (ITR=4) after one pass rolling and found that when the rolling temperature was 400 °C and the reduction ratio was 40%, the bonding strength of Al/Mg/Al laminates was the highest, which was close to 20 MPa.

determine the plastic deformation mechanisms of the laminates, IMAI et al [28] carried out finite element analysis on the cold rolling process of a three-layered sheet having a hard inner layer and soft outer layers. It was found that the greater the flow stress difference between the hard layer and the soft layer, the lower the degree of work hardening, and the more obvious the periodical necking. ROOSTAEI et al [29] analyzed the accumulative rolling bonding process of AZ31 Mg alloy by the finite element method and predicted the equivalent plastic strain and shear strain in the thickness direction of the plate. The equivalent plastic strain increased with increasing friction coefficient, and the increase in temperature made the deformation in the thickness direction of the plate more uniform. RAHDARI et al [30] studied the interlaminar continuity of single hard layer laminates by the finite element method. The results showed that in the low-strain region, the thinning range of each layer is basically the same, and the distribution of strain in each layer is basically the same. In the high-strain region, with the difference in thickness ratio and hardness ratio, the hard layer exhibited necking and fracture.

With the increasing demands for light weight and high strength structural components in aerospace and other fields, ensuring the specific strength, specific rigidity and corrosion resistance of Al/Mg/Al laminates while reducing their weight

has attracted much attention. Increasing the proportion of magnesium alloy in the laminates can achieve this goal and has become a hot topic of current research. However, current studies are focused on laminates with the ITR below 10, and there are few studies on laminates with a larger ITR. The effect of reducing the thickness of the Al layer on the properties and microstructure of Al/Mg/Al laminates is not clear. Therefore, based on previous studies, research on Al/Mg/Al laminates with the ITR ranging from 5 to 50 was carried out by combining simulations and typical working condition experiments, and the analysis of the influence of the ITR on the mechanical properties and interfacial bonding properties of laminates was focused on.

# 2 Numerical simulation and experiment

#### 2.1 Numerical simulation

To study the effect of the ITR on the microstructure and properties of Al/Mg/Al laminates, simulations and experiments were carried out with 1060 industrially pure aluminum in the H24 state and AZ31B magnesium alloy in the rolled state as raw materials. The chemical compositions of the materials are listed in Table 1. Considering that the billets of Al/Mg/Al laminates are stacked symmetrically, the model can be simplified to a two-dimensional symmetrical model, ignoring the temperature difference in the width direction of the roll and width spread of the plates. The roll was regarded as a thermally conductive rigid body, and the whole model was simplified to a plane strain model [31]. The thermal-mechanical coupling models of the Al/Mg/Al laminate hot rolling process were established by commercial finite element method software, as shown in Fig. 1.

In the process of finite element simulation, the anisotropy of the materials was ignored and set as isotropic elastic-plastic materials. Due to the nonlinearity of the materials, the true stress—true strain curves of 1060 aluminum (selected in the literature [32]) and AZ31B magnesium alloy

**Table 1** Chemical compositions of AZ31B Mg alloy and 1060 pure Al (wt.%)

Material	Mg	Cu	Mn	Zn	Ca	Si	Al	Fe	Ti
AZ31B	Bal.	0.01	0.3	1.1	0.04	0.07	2.9	-	_
1060 Al	< 0.03	0.008	< 0.03	< 0.05	_	0.045	Bal.	0.239	0.018

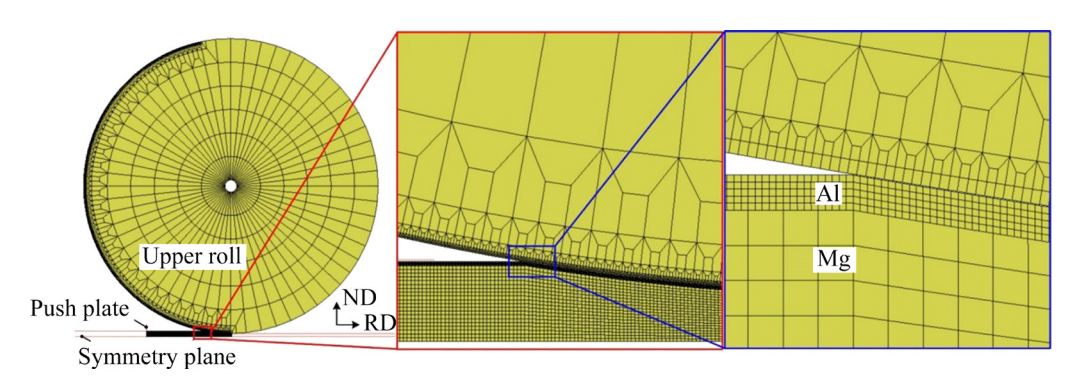


Fig. 1 Rolling finite element model of Al/Mg/Al laminates

(selected in the literature [33]) at different strain rates and temperatures were imported into the Marc material library through the secondary development of the material library. The thermophysical parameters of 1060 aluminum were selected from the literature [32,34]. The thermophysical parameters of AZ31B magnesium alloy were selected from the literature [33]. The thermophysical parameters of the roll material (9Cr2Mo) were selected from the literature [35]. In the simulation analysis, the interface was set to friction contact, and the Coulomb bilinear model was used to simulate the actual rolling condition. The initial temperature of the Al/Mg/Al laminate was set to be 400 °C. The friction coefficients between the roll and the rolled piece and between the magnesium layer and aluminum layer were 0.3. The contact heat transfer coefficient between the roll and the rolled piece was 10 mW/(mm<sup>2</sup>·K). The contact heat transfer coefficient between the aluminum layer and magnesium layer was 15 mW/(mm<sup>2</sup>·K). The rolling process parameters are listed in Table 2, and the simulation condition parameters are shown in Table 3.

Table 2 Rolling process parameters

Simulation parameter	Value
Roll diameter/mm	245
Initial thickness of laminates/mm	8.4
Reduction ratio/%	40
Rolling speed/(rad·s <sup>-1</sup> )	1

At the beginning of the rolling process, the increase in friction stress is beneficial to the tearing of the oxide film on the metal surface and the exposure of fresh metal, thereby promoting the

interfacial bonding strength. By analyzing the simulation results of the contact friction stress in the rolling deformation zone, the deformation zone can be divided into a backward slip zone and forward slip zone during the rolling process of Al/Mg/Al laminates with different ITRs. For the Mg layer, the backward slip zone can be divided into a bite stage and shearing stage. Figure 2 shows a schematic diagram of the rolling deformation zone in the rolling process and indicates the contact friction stress direction in the deformation zone. In Fig. 2, it can be seen that in the bite stage, the contact friction stress is low, the Al layer deforms rapidly, and the Mg layer basically does not deform. The main deformation mode is the yield of the Al layer. In the shearing stage, the contact friction stress increases rapidly, and the tearing degree of the Mg-Al contact surface increases under the shearing effect [36]. When the contact friction stress and the length of the shearing stage increase, the interfacial shearing effect increases and the action time becomes longer, which is conducive to interfacial bonding. In the forward slip zone, the deformation of the Al layer decreases, while the deformation of the Mg layer continues. At the beginning of the forward slip zone, the contact friction stress at the interface is zero, which means that metals pass through the neutral point. When the thickness ratio between layers is constant, it is considered that the interface starts to bond and this point can be regarded as the starting bonding point. According to the volume constancy for each layer, when the thickness ratio between layers is constant in the rolling process, the velocity between layers is the same, and the contact friction stress is zero. An increase in the forward slip zone length can provide

**Table 3** Simulation condition parameters

Working condition	ITR	Reduction ratio/%	Thickness of upper 1060 Al layer/mm	Thickness of AZ31B layer/mm	Thickness of lower 1060 Al layer/mm
1-5-1	5	40	1.20	6.00	1.20
1-10-1	10	40	0.70	7.00	0.70
1-15-1	15	40	0.50	7.40	0.50
1-20-1	20	40	0.38	7.64	0.38
1-30-1	30	40	0.26	7.88	0.26
1-40-1	40	40	0.20	8.00	0.20
1-50-1	50	40	0.16	8.08	0.16

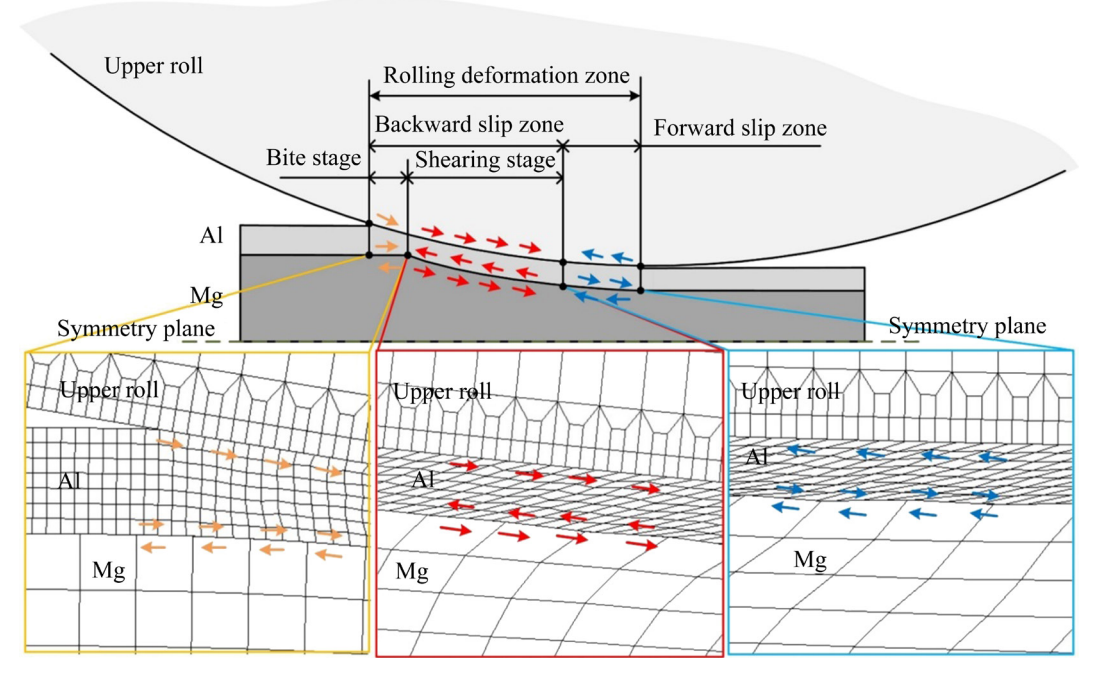


Fig. 2 Schematic diagram of rolling deformation zone (Arrow direction represents contact friction stress direction)

a longer action time for the relative bonding. With an increase in the relative bonding length, the time of the bonded laminates under the interfacial stress is longer, which is more conducive to interfacial bonding [37].

The simulation results at the interface of the rolling deformation zone of Al/Mg/Al laminates with large thickness ratios are shown in Fig. 3. Figure 3 shows that when the ITR increases from 5 to 20, the contact normal stress of the Mg layer, the contact friction stress of the Mg layer and mean equivalent strain of Al and Mg layers at the interface of the deformation zone increase significantly. However, when the ITR is greater than 20, the stress of the Mg layer at the interface of the deformation zone does not increase significantly, and the mean equivalent strain of the Al layer at the interface decreases.

# 2.2 Experiments

According to the typical deformation characteristics in the above simulation, working conditions 1-5-1 (ITR=5), 1-20-1 (ITR=20), and 1-40-1 (ITR=40) were selected for the rolling experiment. The experimental process parameters were the same as those in the simulation. The oxides and dirt on the plate surface were removed before rolling. The treated laminates were subjected to the stacking sequence of 1060 Al-AZ31B Mg-1060 Al and kept in a vacuum tube furnace at 400 °C for 30 min. The Al/Mg/Al laminates were rolled by a two-high rolling mill with a roll diameter of 245 mm at a rolling speed of 1 rad/s. A schematic diagram of the rolling process is shown in Fig. 4.

The metallographic specimens were cut at the middle of the prepared Al/Mg/Al laminates, and

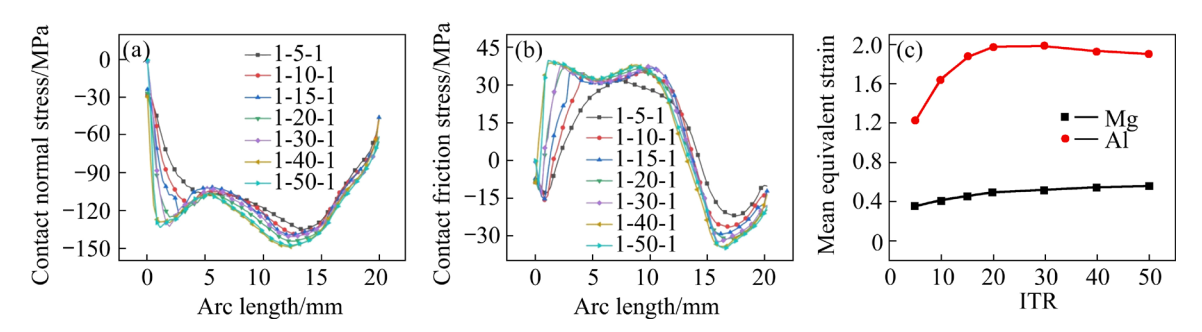


Fig. 3 Simulation results at interface of rolling deformation zone of Al/Mg/Al laminates: (a) Contact normal stress of Mg layer; (b) Contact friction stress of Mg layer; (c) Mean equivalent strain

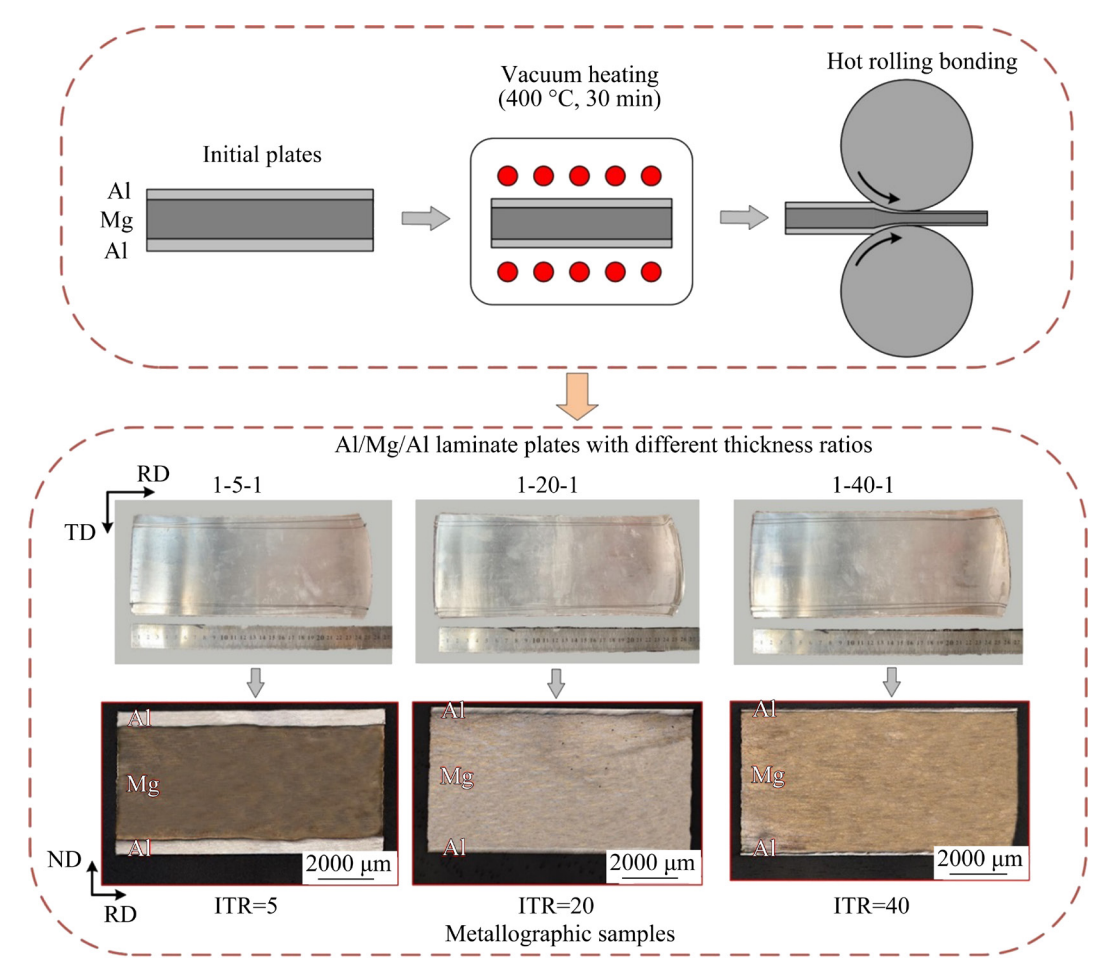


Fig. 4 Schematic diagram showing rolling process of large thickness ratio Al/Mg/Al laminates

then the surface was ground with sandpaper and polished to a mirror with alumina polishing fluid. According to the standards of GB/T 228.1—2010, the tensile specimens were prepared along the rolling direction. The tensile tests and peeling tests were carried out at room temperature using an Instron Series 5969 universal testing machine (Instron Ltd., Norwood, MA, USA). The tensile rate was 0.5 mm/min and the peeling rate was 5 mm/min. Scanning electron microscope (SEM,

JOE IT500, JEOL Ltd., Tokyo, Japan) with energy dispersive spectrometer (EDS) and electron back-scatter diffraction (EBSD) was used to observe the microstructure and tensile fracture morphology of the interface.

The average thicknesses of the constituent metals in the simulation and experiment were determined by measuring the samples at five different locations. The variations in the constituent metal thicknesses are shown in Table 4. The relative errors between the simulation calculation and experimental results are within 10%.

Figure 5 shows the variation in the proportion of the rolled Mg layer with the proportion of the initial Mg layer and the reduction ratio of the component metals after rolling under different working conditions. It can be clearly observed from Fig. 5(a) that when the proportion of the initial Mg layer is higher than 71.4%, the proportion of the rolled Mg layer is approximately linear with that before rolling, that is, when the ITR is higher than 5, the thickness ratio of the component metal layer after rolling is approximately linear with that before

**Table 4** Comparison of simulation and experimental thicknesses of Al layer after rolling

Working condition	Reduction ratio/ %	Experimental thickness/	Simulation thickness/ mm	Relative error/ %
1-5-1	40	0.577	0.641	9.98
1-20-1	40	0.213	0.203	4.69
1-40-1	40	0.120	0.115	4.17

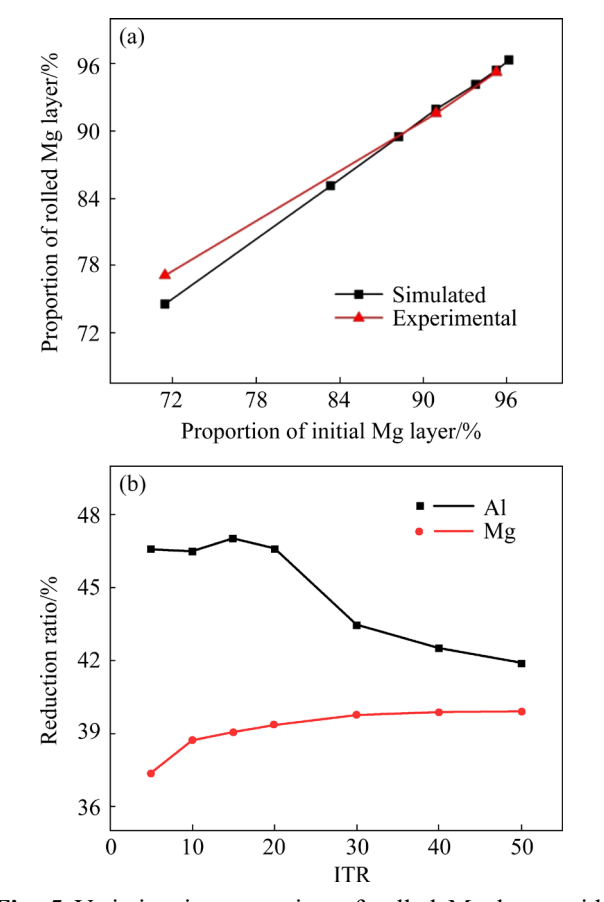


Fig. 5 Variation in proportion of rolled Mg layer with proportion of initial Mg layer (a), and reduction ratio of component metals (b)

rolling. Therefore, the thickness ratio of the metal before rolling can be determined according to the required thickness ratio of the laminates. The thickness reduction ratio of the Al layer is significantly higher than that of the Mg layer when the ITR is 5, as shown in Fig. 5(b). The thickness reduction ratio of the Al layer decreases with increasing ITR, while that of the Mg layer increases. This phenomenon can be explained by the fact that after the Al layer becomes thinner, the Al layer enters the difficult deformation zone, resulting in a decrease in the thickness reduction ratio of the Al layer. The reduction ratio of the Al layer and Mg layer gradually tends to the total reduction ratio (40%) with increasing ITR.

# 3 Results and discussion

#### 3.1 Interfacial structure

SEM images near the interface under different ITRs are shown in Fig. 6. There are no defects such as holes and cracks at the interface, indicating that when the reduction ratio is 40%, the Al/Mg/Al laminates studied in this work have a good bonding interface. Through element line scanning analysis of samples with different ITRs, an obvious diffusion zone can be seen at the interface between the Mg layer and Al layer. From the AZ31B Mg side to the 1060 Al side, the concentration of Mg decreases gradually while the concentration of Al increases gradually. Under the working conditions of 1-5-1, 1-20-1, and 1-40-1, the thicknesses of the interface diffusion layer are the same (3 μm).

#### 3.2 Mechanical properties

The mechanical properties of rolled Al/Mg/Al laminates under working conditions 1-5-1, 1-20-1, and 1-40-1 were tested. The tensile properties of rolled Al/Mg/Al laminates are shown in Fig. 7. The dimensions of tensile specimen are embedded in Fig. 7(a). As shown in Fig. 7, the ultimate tensile strength (UTS) and yield strength (YS) of 1-20-1 are clearly higher than those of 1-5-1, but slightly lower than those of 1-40-1. The elongation (EL) reaches the peak value (23.32%) under the working condition of 1-20-1, showing the best comprehensive mechanical properties.

### 3.3 Interfacial bonding strength

As can be seen from the tensile results, under the working condition of 1-20-1, the laminates

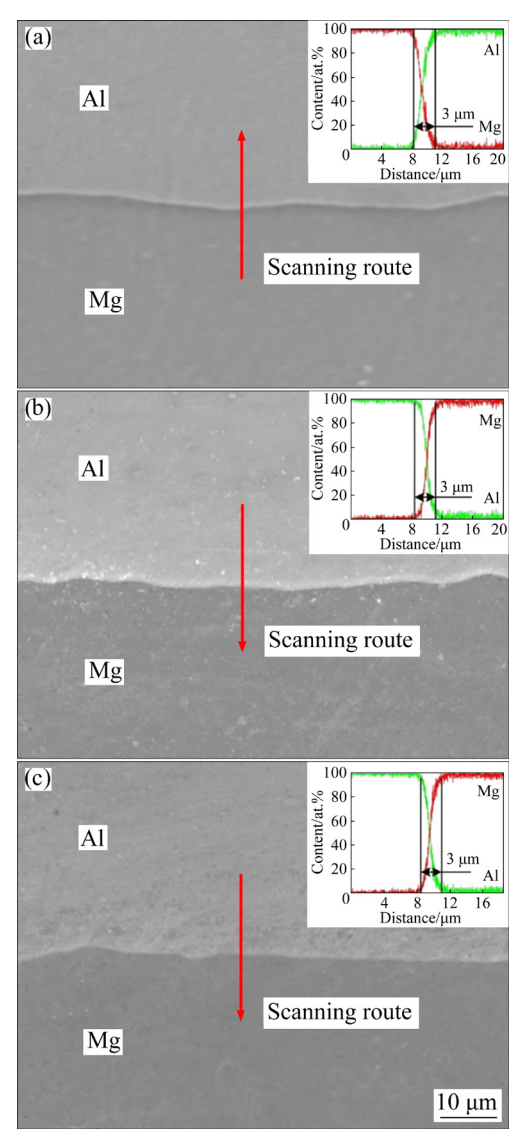


**Fig. 6** SEM images and line scan distribution of samples under different working conditions: (a) 1-5-1; (b) 1-20-1; (c) 1-40-1

show the best comprehensive mechanical properties. According to the previous analysis, the interface plays a role in strengthening and toughening. Therefore, peeling tests of Al/Mg/Al laminates under different working conditions were carried out, and the results are shown in Fig. 8. The dimensions of peeling specimen are embedded in (Fig. 8(b)). Because the thickness of the Al layer after rolling is too thin, under the working conditions of 1-20-1 and 1-40-1, the aluminum matrices exhibit different degrees of tearing at the later stage of the peeling tests (Fig. 8(a)), resulting in inaccurate data at the later stage. Therefore, the average peel strength counts only the data of all peeling sections of the aluminum matrices (Fig. 8(b)). On the statistical

data section, the peeling strength has entered the stable section, and the peeling length of the stable section is more than 15 mm. Under the working condition of 1-20-1, the average peel strength reaches the maximum (12.3 N/mm), followed by that under the working condition of 1-5-1.

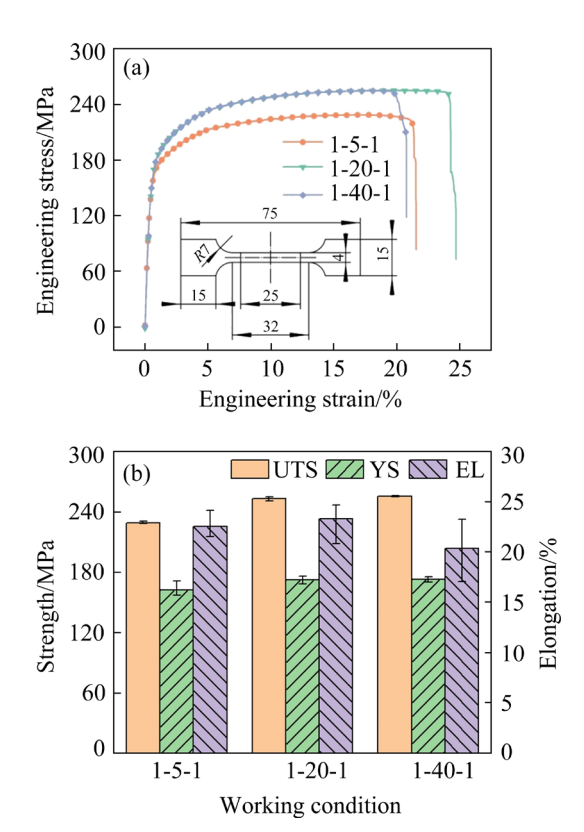
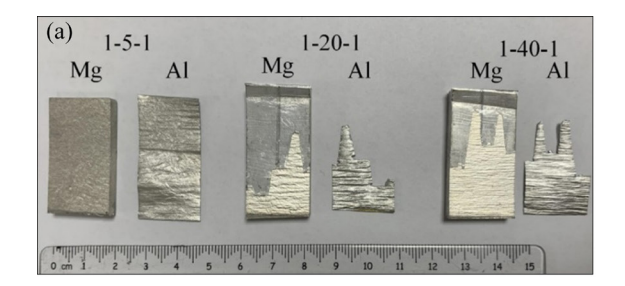


Fig. 7 Engineering stress-strain curves (a) and mechanical properties histograms (b) of samples under different working conditions

To further verify the bonding strength of the laminates, the tensile fractures were quantitatively analyzed. Figure 9 presents the tensile fracture morphologies of samples under different working conditions. Under the working condition of 1-20-1, there is no delamination at the interface after tensile test, while under other two working conditions, there are different degrees of delamination at the interface after tensile test. This phenomenon further indicates that the laminates have the highest interface bonding strength under the working condition of 1-20-1.

#### 3.4 Stress and strain field

To determine the reasons for the changes in the UTS, YS, EL, and bonding strength of Al/Mg/Al laminates with large thickness ratios, the simulation results under working conditions 1-5-1, 1-20-1, and



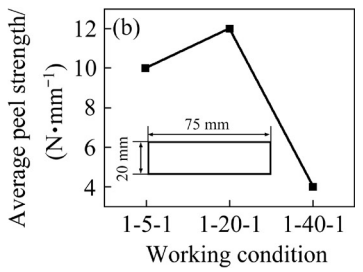
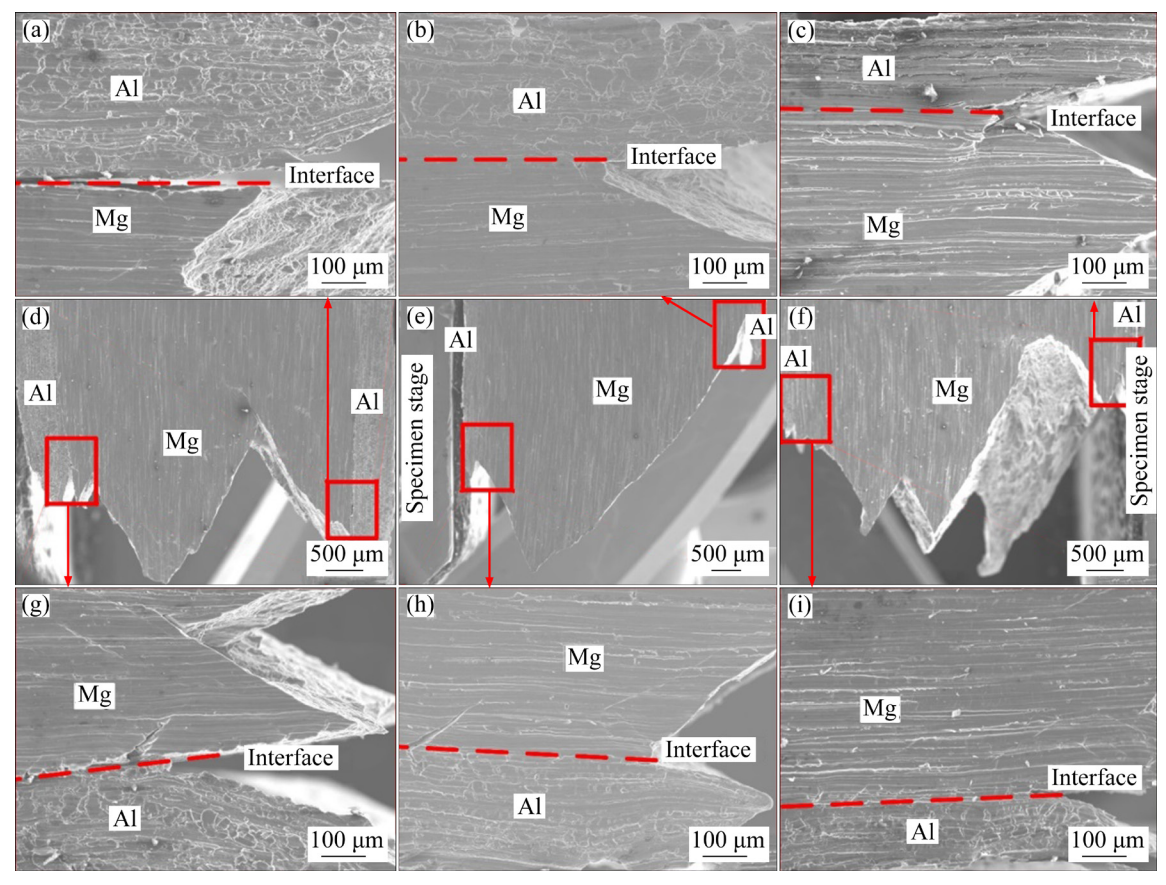


Fig. 8 Peeling test results: (a) Macrographs of peeling samples; (b) Variation in bonding strength (average peel strength) under different working conditions

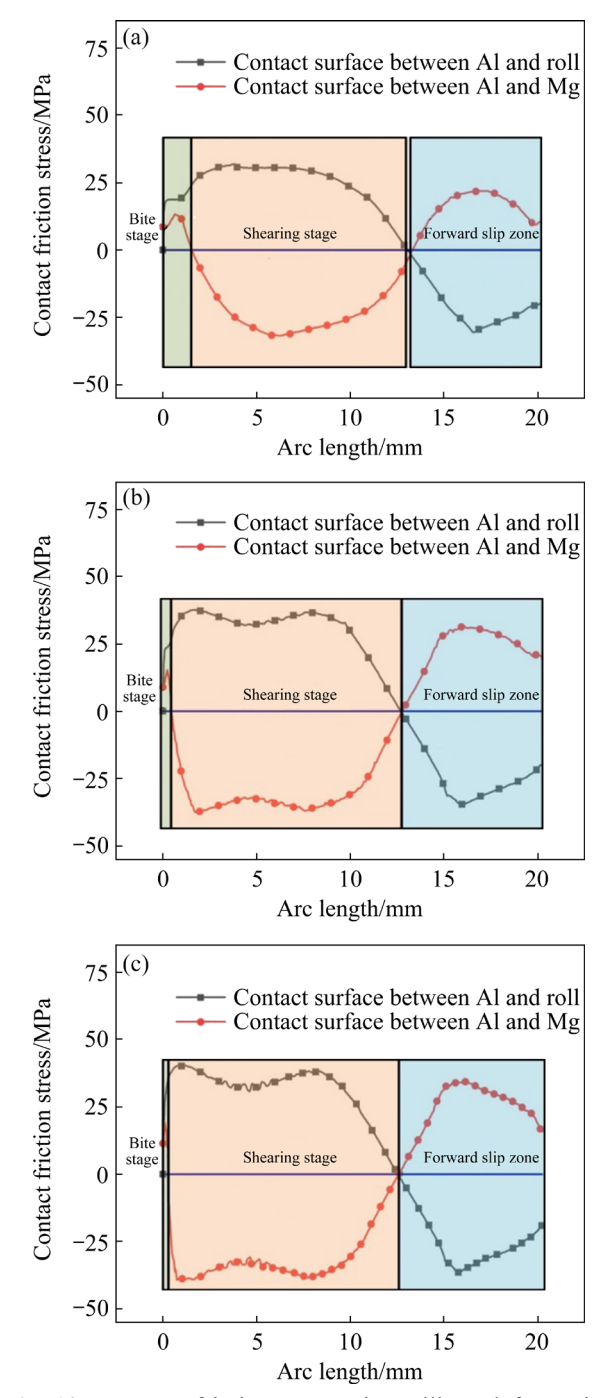


**Fig. 9** Tensile fracture morphologies of samples under different working conditions: (a, d, g) 1-5-1; (b, e, h) 1-20-1; (c, f, i) 1-40-1

1-40-1 were extracted separately. Figure 10 shows the contact friction stress under three working conditions. From Fig. 10, it can be concluded that when the working conditions are 1-5-1, 1-20-1, and 1-40-1, respectively, the length of bite stage is 1.53, 0.47, 0.25 mm, respectively, the length of shearing stage is 11.53, 12.21, 12.31 mm, respectively, and the length of forward slip zone is 6.92, 7.54, 7.66 mm, respectively. With an increase in the ITR, the reason for the increase in the shearing stage length and the forward slip zone length is that with the increase in ITR, the thickness of the aluminum

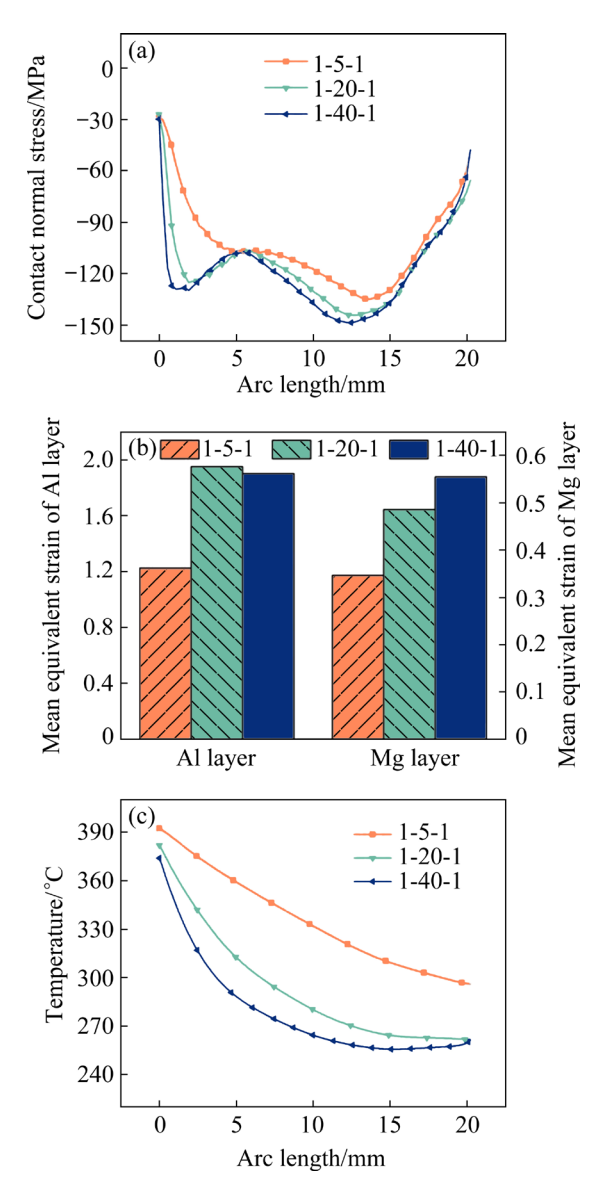
layer is reduced. Under the same rolling conditions, the rolling force is more easily transferred to the interface, the contact normal stress and contact friction stress at the interface increase, and the length of the bite stage decreases. When the total length of the rolling deformation zone is the same, the length of the shearing stage and the length of the forward slip zone increase.

Figure 11 shows stress, strain, and temperature variations under three typical working conditions. Through the simulation results, the reasons for the change in bonding strength of Al/Mg/Al laminates



**Fig. 10** Contact friction stress in rolling deformation zone under different working conditions: (a) 1-5-1; (b) 1-20-1; (c) 1-40-1

with a large thickness ratio can be explained as follows: when the ITR increases from 5 to 20, the contact normal stress, contact friction stress (Fig. 10), mean equivalent strains of the Al layer and Mg layer at the interface in the deformation zone, and length of the forward slip zone (that is, the relative bonding length of the deformation zone) are significantly increased. With increasing interfacial stress and strain, the interfacial bonding



**Fig. 11** Contact normal stress of Mg layer (a), mean equivalent strain of Mg and Al layers (b), and temperature of Al layer (c) at interface of rolling deformation zone under different working conditions

strength increases. When the ITR increases from 20 to 40, the contact normal stress, contact friction stress at the interface, and relative bonding length of the deformation zone are basically unchanged; however, the mean equivalent strain of the Al layer decreases, and the temperature drop degree of the Al layer increases. After the thickness of the Al layer is very thin, the Al layer enters the difficult deformation zone. When the relative bonding length is basically the same, with an increase in the difficult deformation degree of the Al layer, the interfacial tearing degree decreases under the action of the same interfacial friction stress. Then, under

the action of the same interfacial normal stress and relative bonding length of the deformation zone, the bonding strength decreases. The increase in stress and strain at the interface is conducive to improving the interfacial bonding strength. However, when the ITR is higher than 20, the work hardening effect of the Al layer begins to weaken the bonding of the interface, which is not conducive to bonding.

Since the strength of the AZ31B magnesium alloy is higher than that of 1060 industrially pure aluminum, the strength of the laminates can be improved by increasing the thickness of the Mg layer. Therefore, the UTS and YS of Al/Mg/Al laminates with large thickness ratios increase when the ITR increases from 5 to 40. Under the working condition of 1-20-1, although the Al layer is thin, due to the improvement in the interfacial bonding strength between the Al layer and Mg layer, the EL of the laminates increases under the effect of interface strengthening [38]. Under the working condition of 1-40-1, the effect of the Al layer decreases sharply because the thickness of the Al layer is very thin after rolling and the interfacial bonding strengths of laminates decrease. Under this working condition, the performance of Al/Mg/Al laminates with a large thickness ratio mainly depends on the performance of the Mg layer, and the EL decreases significantly.

# 3.5 Microstructure

To observe the microstructure of Al/Mg/Al laminates under the working condition of 1-20-1 during the rolling process, the laminates were

water-cooled immediately after rolling to retain the high temperature deformation structure, and EBSD observations at the interface were carried out. The inverse pole figure (IPF), recrystallized extent, band contrast (BC) map, and grain boundary misorientations at the interface of the Al/Mg/Al laminate under the working condition of 1-20-1 are presented in Fig. 12 and Fig. 13. Figure 12(a) shows that there are obvious shear bands on the Al layer and obvious shear bands composed of fine grains on the Mg layer. According to Fig. 12(b), these fine grains on the Mg layer are recrystallized grains, which means that during the rolling process of the Al/Mg/Al laminate with a large thickness ratio, the large contact friction stress causes higher local shear deformation near the interface [39]. The proportion of deformed grains on the Al layer is very high. As shown in Fig. 13(a), several types of twin boundaries are observed on the Mg layer. The two main twin types are  $\{10\overline{12}\}$  tensile twins and  $\{10\overline{1}1\} - \{10\overline{1}2\}$  secondary compression twins. The Al layer and Mg layer are dominated by low-angle grain boundaries (LAGBs) after water cooling, and the dislocation density is high (Figs. 13(b) and (c)). The misorientation angles on the Mg layer have an obvious peak at approximately 86°, which also proves the existence of tensile twins.

EBSD observations of the Al/Mg/Al laminates after air-cooling under working conditions of 1-5-1, 1-20-1, and 1-40-1 were carried out to further analyze the reasons for the performance change of the laminates. The pole figures (PFs) of the laminates

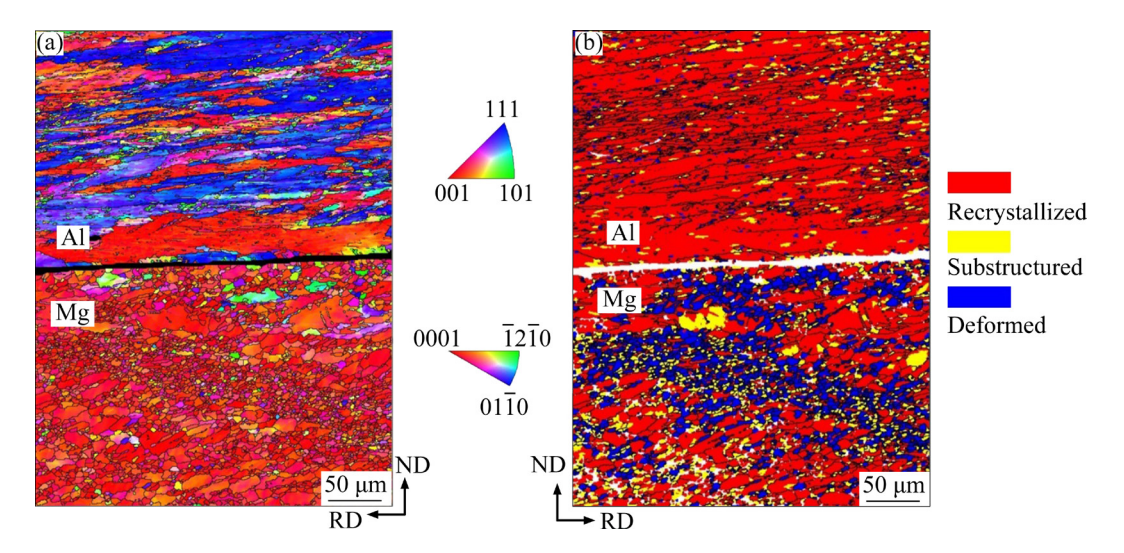


Fig. 12 IPF map (a), and recrystallized extent (b) of Al/Mg/Al laminates under working condition of 1-20-1 after water-cooling

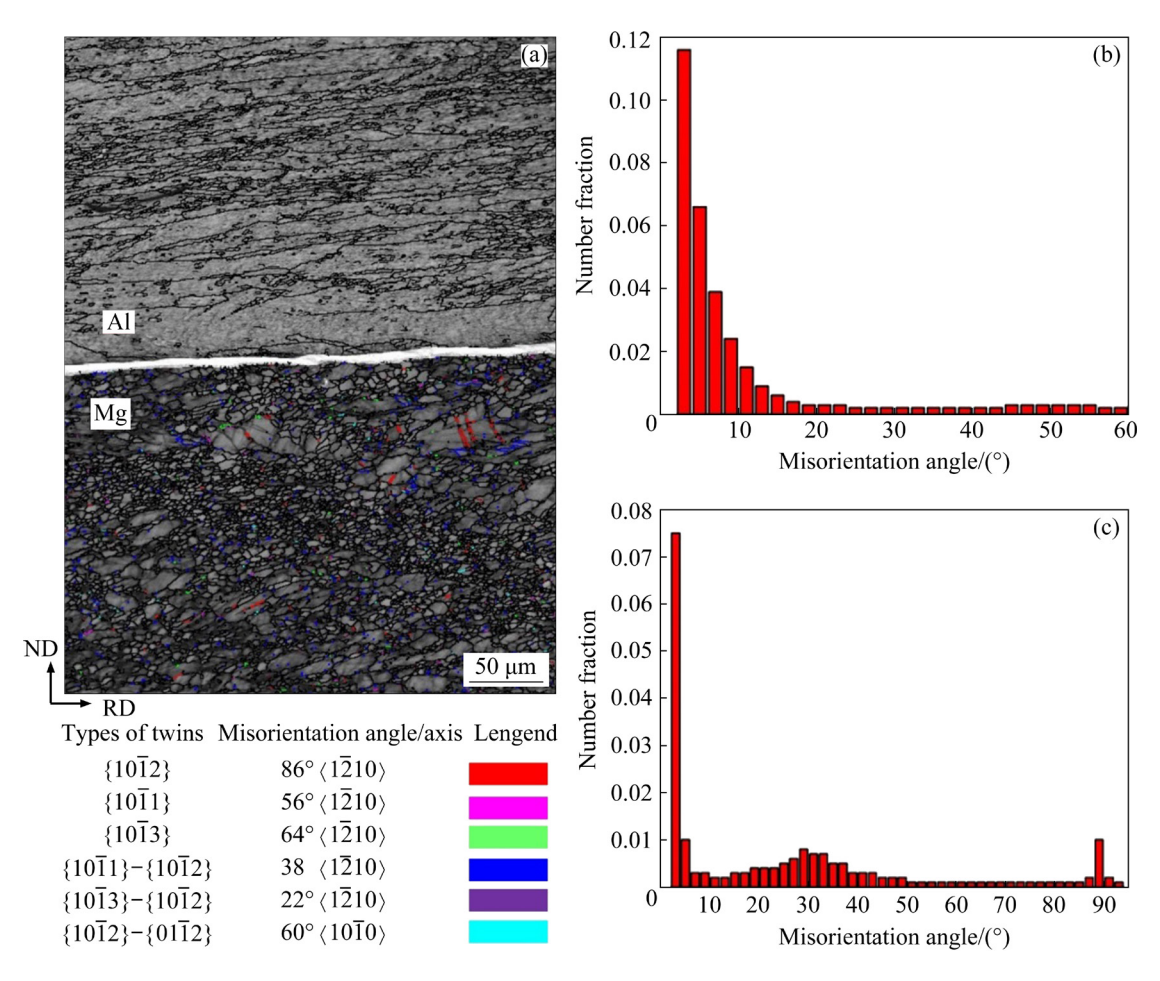


Fig. 13 BC map (a), grain boundary misorientations of Al (b), and Mg (c) layers in Al/Mg/Al laminates under working condition of 1-20-1 after water-cooling

under different working conditions are shown in Fig. 14. Under the working condition of 1-5-1, the Al layer mainly presents a typical  $\{112\}\langle 111\rangle$ copper texture, which is stable and common in the FCC metals, especially in FCC metals with high stacking fault energy, such as Al [40]. When the ITR increases to 20 and 40, the textures of the Al layer change into shear texture. With an increase in the ITR, the contact friction stress of the interface and the length of the shearing stage increase (Fig. 10), and then the shear effect on the Al layer increases. This shows that when the ITR reaches 20, the shear deformation of the Al layer passes through the interface, and the grains near the interface exhibit a certain angle with the interface, forming a shear band and then forming a shear texture. The  $\{111\}\langle 110 \rangle$  and  $\{111\}\langle 112 \rangle$  components in shear texture can improve the plastic strain ratio [41]. The dominant role of shear texture in the Al layer suggests that continuous recrystallization occurs in the Al layer [42]. Under three different working conditions studied in this work, the c-axis of Mg layer grains near the interface is parallel to ND, which is a typical (0001) basal texture. Under the working condition of 1-20-1, the basal texture is elongated along RD, indicating that the c-axis tilts from ND to RD, which can be attributed to the activation of the  $\langle c+a \rangle$  non-basal slip system. The activation of the  $\langle c+a \rangle$  non-basal slip system helps to explain the increase in the EL of the laminates [43].

The IPFs of Al/Mg/Al laminates are shown in Fig. 15. Due to the large thickness ratio of Al/Mg/Al laminates in the rolling process, the contact stress at the interface and the internal storage energy are high. In the air-cooling process, driven by the internal stored energy, the grains in the deformation process basically transform into recrystallized grains. With an increase in the ITR, the grain size of the Al layer and Mg layer decreases, and the shear bands of the Al layer are more obvious. Under the working condition of

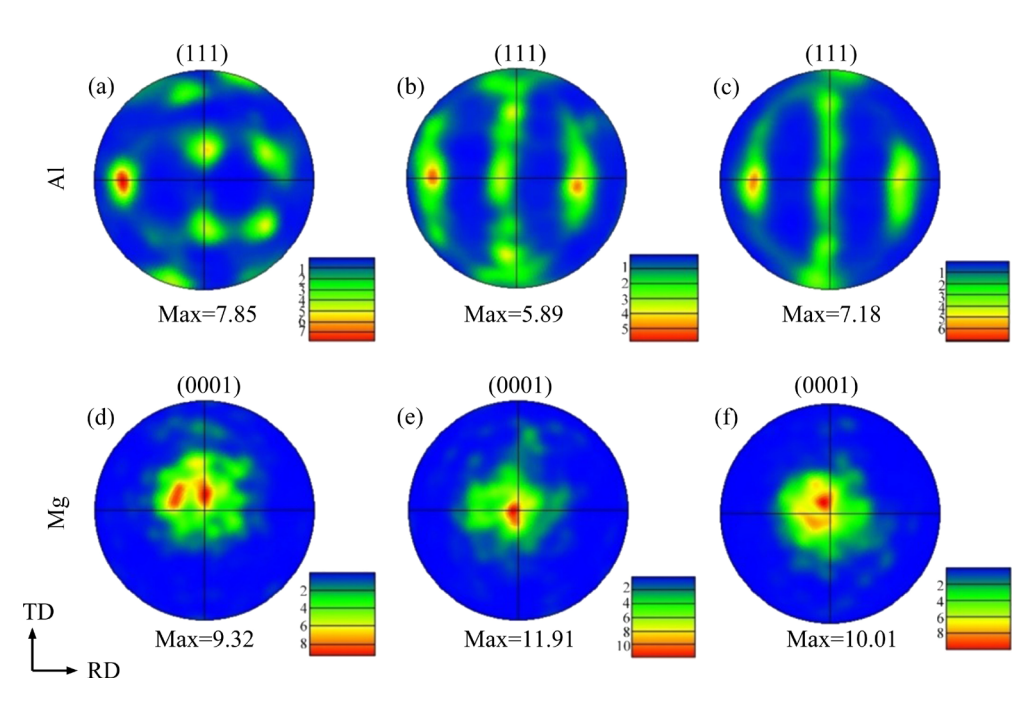


Fig. 14 PF maps of Al/Mg/Al laminates under different working conditions: (a, d) 1-5-1; (b, e) 1-20-1; (c, f) 1-40-1

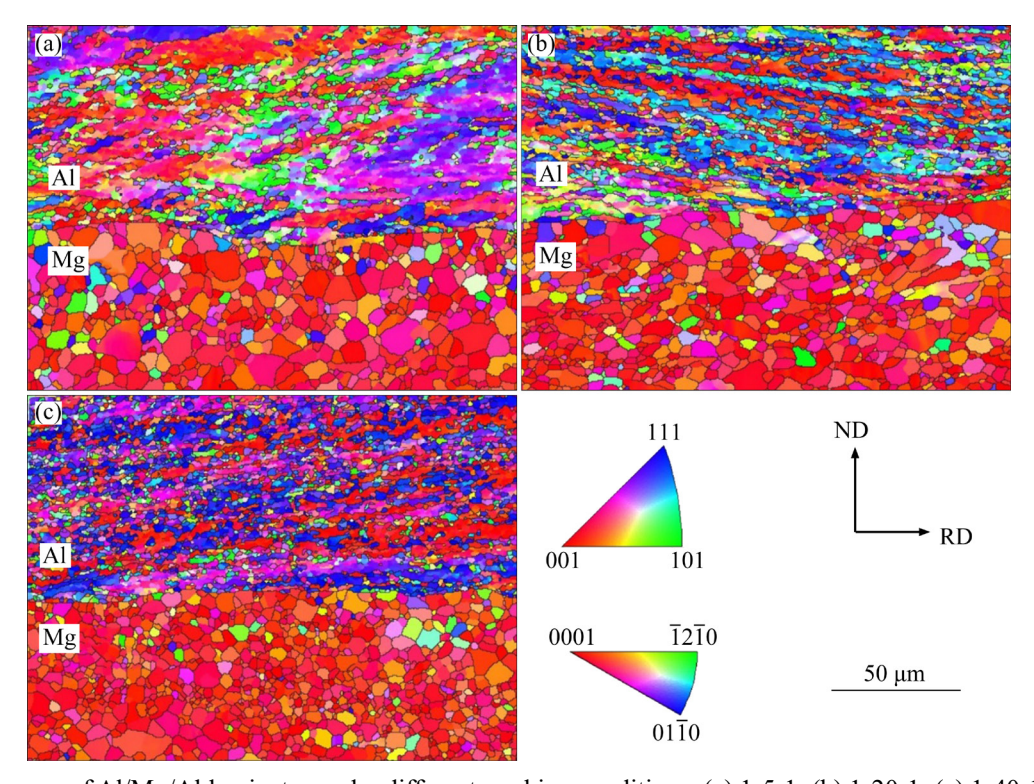


Fig. 15 IPF maps of Al/Mg/Al laminates under different working conditions: (a) 1-5-1; (b) 1-20-1; (c) 1-40-1

1-20-1, shear bands can also be clearly observed on the Mg layer. This phenomenon can be explained by the increase in the contact friction stress at the interface (Fig. 10), and the shear effect at the interface is enhanced. A better shear texture on the Al layer can give rise to finer grains [44]. According to the Hall–Petch relationship, the finer the grain size is, the higher the strength and ductility of the material are, which also helps to explain why the strength of the laminates increases with increasing ITR (Fig. 7). Although the ductility of the Mg layer and Al layer is improved under the working condition of 1-40-1, due to the decrease in the interfacial bonding strength and the thin Al layer,

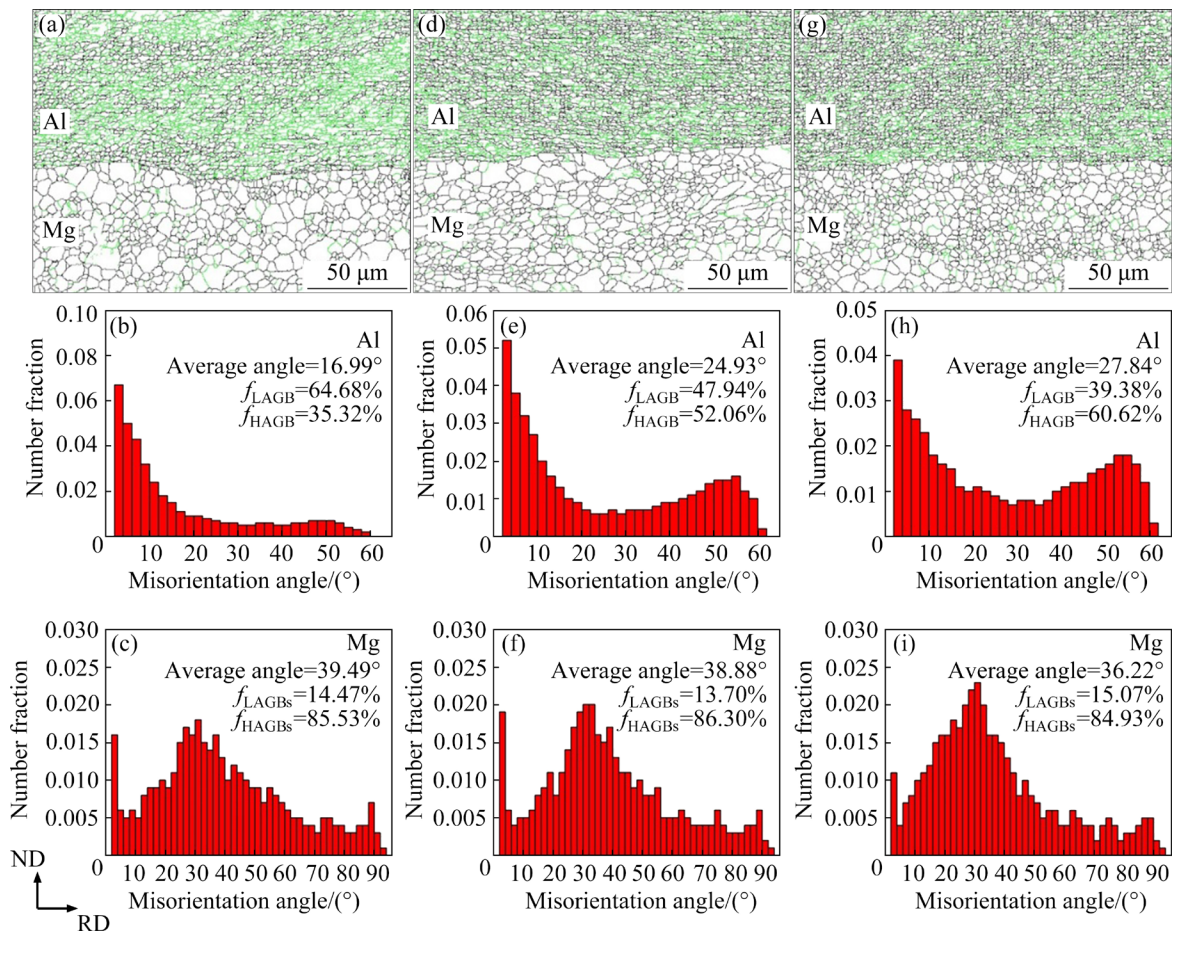
the mechanical properties of the laminates depend mainly on the properties of the Mg layer, and then the EL decreases.

Figure 16 shows the grain boundaries and misorientations of the Al/Mg/Al laminates. As shown in Figs. 16(b, e, h), with increasing ITR, the proportion of high-angle grain boundaries (HAGBs) on the Al layer increases, which indicates that the dislocation density decreases and the recovery initiates [40]. Under the working condition of 1-20-1, the HAGBs on the Mg layer account for the largest proportion.

The peak value at 5° represents the range of the sub-grains of the elongated grains that have not been recrystallized. The large probability of the peak value at 30° is due to the 30° (0001) misorientation relationship commonly existing in the process of recrystallized grain growth of HCP materials, and its strength is related to the fraction of recrystallized grains [45]. When the ITR increases from 5 to 40, the peak strength at 5° in the

Mg layer decreases (Fig. 16(c, f, i)), while the peak strength of the grain boundary angle at  $30^{\circ}$  increases, suggesting that the elongated grains in the Mg layer are replaced by equiaxed grains. The emergence of twins and the activation of  $\langle c+a \rangle$  slip also accumulate more stored energy, providing a greater driving force for recrystallization [46]. Although the grains are finer and the recrystallization degree is larger under the working condition of 1-40-1, the ductility of magnesium is still lower than that of aluminum.

The recrystallization fraction of Al/Mg/Al laminates is shown in Fig. 17. With an increase in the ITR, the recrystallization fraction of the Mg layer decreases first and then increases, while the Al layer presents the opposite trend, and the proportion of deformed grains increases first and then decreases in both the Mg layer and Al layer. This confirms that the laminates have the best deformation compatibility between the Al layer and Mg layer under the working condition of 1-20-1.



**Fig. 16** EBSD images showing low-angle (2°-15°, green) and high-angle grains boundaries (>15°, black) (a, d, g) and grain boundary misorientations (b, c, e, f, h, i) under different working conditions: (a, b, c) 1-5-1; (d, e, f) 1-20-1; (g, h, i) 1-40-1

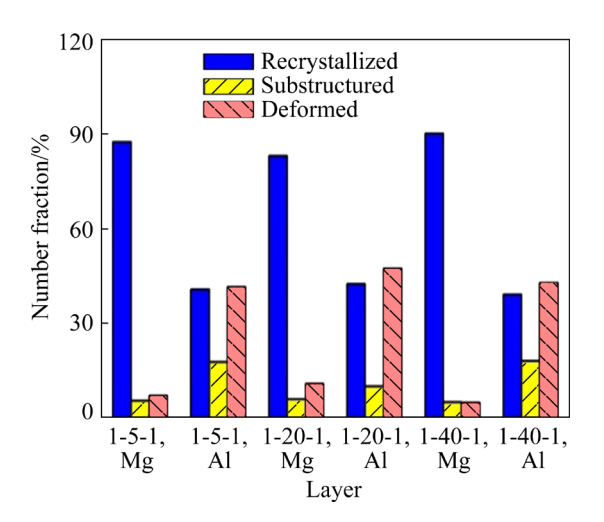


Fig. 17 Recrystallization fraction of Al/Mg/Al laminates

This is consistent with the previously mentioned finding that a higher strain at the interface is beneficial to the deformation. Meanwhile, when the ITR reaches 40, the Al layer is too thin to deform easily, and the deformation ability of the Mg layer also decreases due to the large temperature drop.

#### 4 Conclusions

- (1) Under different working conditions, the thickness ratio after rolling is basically linear with that before rolling so that the ITR can be calculated according to the required thickness ratio. With an increase in the ITR, the reduction ratio of the Al layer gradually decreases, and that of the Mg layer gradually increases, both gradually tending to the total reduction ratio.
- (2) The ultimate tensile strength and yield strength of Al/Mg/Al laminates increase with increasing ITR. The interfacial bonding strength and elongation reach the maximum under the working condition of 1-20-1.
- (3) The contact friction stress, contact normal stress, mean equivalent strain of the Mg layer, and relative bonding length at the interface of the deformation zone increase with the increase of the ITR. Meanwhile, under the working condition of 1-20-1, the mean equivalent strain of the Al layer at the interface reaches the maximum. Under the working condition of 1-40-1, the difficulty of deformation increases, the interfacial bonding strength decreases, and the properties of the magnesium alloy play a dominant role in laminates.
  - (4) For laminates subjected to water-cooling

immediately after rolling, under the working condition of 1-20-1, obvious shear bands composed of recrystallized grains and twins can be clearly observed on the Mg layer. For laminates subjected to air-cooling after rolling, with an increase in the ITR, the texture of the Al layer changes into a shear texture, which can improve the plastic strain ratio. The deformation compatibility is the best under the working condition of 1-20-1.

# **Acknowledgments**

This work was supported by the National Key Research and Development Program of China (No. 2018YFA0707300), the General Program of National Natural Science Foundation of China (No. 51905372), the Key Project of Shanxi Province, China (No. 20181101008), and the Postdoctoral Science Foundation of China (No. 2020T130463).

#### References

- [1] SHARIFI ASL N, MIRSALEHI S E, DEHGHANI K. Effect of TiO<sub>2</sub> nanoparticles addition on microstructure and mechanical properties of dissimilar friction stir welded AA6063-T4 aluminum alloy and AZ31B-O magnesium alloy [J]. Journal of Manufacturing Processes, 2019, 38: 338–354.
- [2] MORDIKE B L, EBERT T. Magnesium: Properties—applications—potential [J]. Materials Science and Engineering A, 2001, 302: 37–45.
- [3] ABEDI R, AKBARZADEH A, HADIYAN B, HASHEMI R. Formability of tri-layered IF240/AZ31/IF240 composite with strong bonding: Experimental and finite element modeling [J]. Journal of Materials Engineering and Performance, 2021, 30(11): 8402–8411.
- [4] HOU Cai-hong, YE Zhi-song, QI Fu-gang, WANG Qing, LI Lian-hui, OUYANG Xiao-ping, ZHAO Nie. Effect of Al addition on microstructure and mechanical properties of Mg-Zn-Sn-Mn alloy [J]. Transactions of Nonferrous Metals Society of China, 2021, 31(7): 1951–1968.
- [5] NIE Hui-hui, ZHENG Liu-wei, KANG Xiao-ping, HAO Xin-wei, LI Xian-rong, LIANG Wei. In-situ investigation of deformation behavior and fracture forms of Ti/Al/Mg/Al/Ti laminates [J]. Transactions of Nonferrous Metals Society of China, 2021, 31(6): 1656–1664.
- [6] YANG Rui, MA Wei, WANG Chao, WANG Ting-mei, WANG Qi-hua. Effect of hot rolling on microstructure and tribology behaviors of Ti-50.8Ni alloy [J]. Transactions of Nonferrous Metals Society of China, 2021, 31(4): 967–979.
- [7] LI Xian-rong, LIANG Wei, ZHAO Xing-guo, ZHANG Yan, FU Xiao-peng, LIU Fen-cheng. Bonding of Mg and Al with Mg-Al eutectic alloy and its application in aluminum coating on magnesium [J]. Journal of Alloys and Compounds, 2009, 471(1/2): 408-411.
- [8] ATIFEH S M, ROUZBEH A, HASHEMI R, SEDIGHI M. Effect of annealing on formability and mechanical properties

- of AA1050/Mg-AZ31B bilayer sheets fabricated by explosive welding method [J]. The International Journal of Advanced Manufacturing Technology, 2022, 118: 775–784.
- [9] HU Jian-jun, LIAO Jing, YANG Xian, ZENG Jing, LI Hui, SONG Bo, XU Hong-bin, GUO Ning, JIN Yan. Microstructure and properties of Al-coating on AZ31 magnesium alloy prepared by pack-cementation [J]. Transactions of Nonferrous Metals Society of China, 2022, 32(2): 493–502.
- [10] LIU Ke, LOU Feng, FU Jun-jian, YU Zi-jian, LI Shu-bo, WANG Zhao-hui, DU Xian, DU Wen-bo. Microstructure and corrosion behaviors of as-rolled Mg-Zn-Er alloy sheets [J]. Transactions of Nonferrous Metals Society of China, 2022, 32(6): 1881–1895.
- [11] PAHLAVANI M, RAHMATABADI D, AHMADI M, HASHEMI R. The role of thickness on the fracture behavior of Al/Mg-Li/Al composite processed by cold roll bonding [J]. Materials Science and Engineering A, 2021, 824: 141851.
- [12] ZENG Xiang-yu, WANG Yu-xin, LI Xue-qi, LI Xiao-jie, ZHAO Tie-jun. Effect of inert gas-shielding on the interface and mechanical properties of Mg/Al explosive welding composite plate [J]. Journal of Manufacturing Processes, 2019, 45: 166–175.
- [13] MATSUMOTO H, WATANABE S, HANADA S. Fabrication of pure Al/Mg-Li alloy clad plate and its mechanical properties [J]. Journal of Materials Processing Technology, 2005, 169(1): 9-15.
- [14] TAYYEBI M, RAHMATABADI D, ADHAMI M, HASHEMI R. Influence of ARB technique on the microstructural, mechanical and fracture properties of the multilayered Al1050/Al5052 composite reinforced by SiC particles [J]. Journal of Materials Research and Technology, 2019, 8(5): 4287–4301.
- [15] BI Xiao-lin, HU Yu-jun, LI Rui-feng, ZHAO Hong-jin, LI Tao-tao. A novel method for preparing Al/Mg/Al laminated composite material, processing maps and interface diffusion analysis [J]. Journal of Alloys and Compounds, 2022, 900: 163417.
- [16] WANG Hong-wei, WANG Cui-ju, DENG Kun-kun, NIE Kai-bo, LIANG Wei. Microstructure and mechanical properties of Al/Mg/Al composite sheets containing trapezoidal shaped intermediate layer [J]. Materials Science and Engineering A, 2021, 811: 140989.
- [17] WANG Peng-ju, CHEN Ze-jun, HU Chao, LI Bo-xin, MO Tai-qian, LIU Qing. Effects of annealing on the interfacial structures and mechanical properties of hot roll bonded Al/Mg clad sheets [J]. Materials Science and Engineering A, 2020, 792: 139673.
- [18] CHEN Liang, TANG Jian-wei, ZHAO Guo-qun, ZHANG Cun-sheng, CHU Xing-rong. Fabrication of Al/Mg/Al laminate by a porthole die co-extrusion process [J]. Journal of Materials Processing Technology, 2018, 258: 165–173.
- [19] TANG Jian-wei, CHEN Liang, ZHAO Guo-qun, ZHANG Cun-sheng, SUN Lu. Achieving three-layered Al/Mg/Al sheet via combining porthole die co-extrusion and hot forging [J]. Journal of Magnesium and Alloys, 2020, 8(3): 654–666.
- [20] JIANG Zai-liang, FAN Zi-tian, JIANG Wen-ming, LI

- Guang-yu, WU Yao, GUAN Feng, JIANG Hai-xiao. Interfacial microstructures and mechanical properties of Mg/Al bimetal produced by a novel liquid—liquid compound casting process [J]. Journal of Materials Processing Technology, 2018, 261: 149–158.
- [21] WANG Juan, LI Ya-jiang, LIU Peng, GENG Hao-ran. Microstructure and XRD analysis in the interface zone of Mg/Al diffusion bonding [J]. Journal of Materials Processing Technology, 2008, 205(1/2/3): 146–150.
- [22] WU Chuang-song, WANG Tao, SU Hao. Material flow velocity, strain and strain rate in ultrasonic vibration enhanced friction stir welding of dissimilar Al/Mg alloys [J]. Journal of Manufacturing Processes, 2022, 75: 13–22.
- [23] ZHAO Ya-dong, LU Yao-wen, LUO Ya-long, HE Yang-yang, GUO Xue-feng, CUI Hong-bao, WANG Shu-guang, WANG Zhi-gang. Microstructure evolution and fracture behavior of dissimilar friction stir welding of 1060Al alloy to AZ31B Mg alloy [J]. Materials Characterization, 2021, 180: 111440.
- [24] ZHANG Ting-ting, WANG Wen-xian, ZHANG Wei, ZHOU Jun, YAN Zhi-feng. Interfacial microstructure evolution and deformation mechanism in an explosively welded Al/Mg alloy plate [J]. Journal of Materials Science, 2019, 54(12): 9155–9167.
- [25] CHEN Ze-jun, ZENG Zhen, HUANG Guang-jie, LIU Qing. Research on the Al/Mg/Al three-layer clad sheet fabricated by hot roll bonding technology [J]. Rare Metal Materials and Engineering, 2011, 40: 136–140.
- [26] ZHANG X P, YANG T H, CASTAGNE S, WANG J T. Microstructure; bonding strength and thickness ratio of Al/Mg/Al alloy laminated composites prepared by hot rolling [J]. Materials Science and Engineering A, 2011, 528(4/5): 1954–1960.
- [27] WEI Ai-li, LIU Xing-hai, DONG Li, LIANG Wei. Binding property of Al/Mg/Al thin plates fabricated by one-pass hot rolling with different reduction ratios, temperatures and annealing treatments [J]. Rare Metals, 2018, 37(2): 136–142.
- [28] IMAI T, UTSUNOMIYA H, MATSUMOTO R. Finite element analysis of plastic instability phenomenon in cold rolling of clad sheets [J]. Procedia Engineering, 2017, 184: 306–312.
- [29] ROOSTAEI A A, ZAREI-HANZAKI A, PARSA M H, FATEMI-VARZANEH S M. An analysis to plastic deformation behavior of AZ31 alloys during accumulative roll bonding process [J]. Journal of Materials Science, 2010, 45(16): 4494–4500.
- [30] RAHDARI M, REIHANIAN M, BAGHAL S M L. Microstructural control and layer continuity in deformation bonding of metallic laminated composites [J]. Materials Science and Engineering A, 2018, 738: 98–110.
- [31] KOBAYASHI S, OH S, ALTAN T, Chaudhary A. Metal forming and the finite-element method [J]. Journal of Materials Shaping Technology, 1990, 8: 65.
- [32] ZHAN Li-hua. Rheological behavior research and thermomechanical coupled analysis of aluminium continuous roll casting process [D]. Changsha: Central South University, 2005. (in Chinese)
- [33] WANG Yue-lin. Numerical simulation and experimental

- study on roll forming of Mg/Al composite sheets by corrugated roll [D]. Taiyuan: Taiyuan University of Technology, 2019. (in Chinese)
- [34] HUANG Hua-gui, LIU Wen-wen, WANG Wei, DU Feng-shan. Thermal-mechanical coupled modelling and numerical simulation for twin-roller casting process with technique of deactivate and reactivate element [J]. China Mechanical Engineering, 2015, 26(11): 1503–1508. (in Chinese)
- [35] CAI Ban. Research on 2 high mill rolls in induction heating process [D]. Shenyang: Northeastern University, 2012. (in Chinese)
- [36] WANG Tao, LIU Wen-li, LIU Yuan-ming, WANG Zhen-hua, IGNATOV A V, HUANG Qing-xue. Formation mechanism of dynamic multi-neutral points and cross shear zones in corrugated rolling of Cu/Al laminated composite [J]. Journal of Materials Processing Technology, 2021, 295: 117157.
- [37] REZAII A, SHAFIEI E, OSTOVAN F, DANESHMANESH H. Experimental & theoretical investigation of roll bonding process of multilayer strips by finite element method [J]. Journal of Manufacturing Processes, 2020, 54: 54–69.
- [38] ABEDI R, AKBARZADEH A. Bond strength and mechanical properties of three-layered St/AZ31/St composite fabricated by roll bonding [J]. Materials & Design, 2015, 88: 880–888.
- [39] WANG Tao, WANG Yue-lin, BIAN Li-ping, HUANG Qing-xue. Microstructural evolution and mechanical behavior of Mg/Al laminated composite sheet by novel corrugated rolling and flat rolling [J]. Materials Science and Engineering A, 2019, 765: 138318.

- [40] NIE Hui-hui, LIANG Wei, CHEN Hong-sheng, ZHENG Liu-wei, CHI Cheng-zhong, LI Xian-rong. Effect of annealing on the microstructures and mechanical properties of Al/Mg/Al laminates [J]. Materials Science and Engineering A, 2018, 732: 6–13.
- [41] KIM K H, LEE D N. Analysis of deformation textures of asymmetrically rolled aluminum sheets [J]. Acta Materialia, 2001, 49: 2583–2595.
- [42] JAMAATI R, TOROGHINEJAD M R. Effect of stacking fault energy on deformation texture development of nanostructured materials produced by the ARB process [J]. Materials Science and Engineering A, 2014, 598: 263–276.
- [43] AGNEW S R, YOO M H, TOME C N. Application of texture simulation to understanding mechanical behavior of Mg and solid solution alloys containing Li or Y [J]. Acta Materialia, 2001, 49(20): 4277–4289.
- [44] LEE J K, LEE D N. Texture control and grain refinement of AA1050 Al alloy sheets by asymmetric rolling [J]. International Journal of Mechanical Sciences, 2008, 50(5): 869–887.
- [45] HIRSCH J, AL-SAMMAN T. Superior light metals by texture engineering: Optimized aluminum and magnesium alloys for automotive applications [J]. Acta Materialia, 2013, 61(3): 818–843.
- [46] NIE Hui-hui, LIANG Wei, ZHENG Liu-wei, REN Xiao-xia, CHI Cheng-zhong, FAN Hai-wei. The microstructure, texture and mechanical properties of the rolled Al/Mg/Al clad sheets [J]. Journal of Materials Engineering and Performance, 2016, 25(11): 4695–4705.

# 大厚比 AI/Mg/AI 层合板的热轧工艺与性能

李 婷 1,2,3, 王 涛 1,2,3, 刘文文 1,2,3, 黄志权 4, 姜正义 3, 黄庆学 1,2,3

- 1. 太原理工大学 机械与运载工程学院,太原 030024;
- 2. 先进金属复合材料成形技术与装备教育部工程研究中心,太原 030024;
  - 3. 太原理工大学 中澳联合研究中心,太原 030024;
    - 4. 太原科技大学 机械工程学院,太原 030024

摘 要:通过热轧工艺制备初始厚度比(单层镁初始厚度与单层铝初始厚度的比值)为 5~40 的 Al/Mg/Al 层合板。采用模拟和实验相结合的方法研究初始厚度比对 Al/Mg/Al 层合板的应力场、应变场、组织演变和性能的影响。结果表明,随着初始厚度比的增加,层合板的极限抗拉强度和屈服强度增加,界面结合强度和伸长率先增加后降低。当初始厚度比为 20 时,大厚比 Al/Mg/Al 层合板具有最佳的综合力学性能,界面结合强度(剥离强度)和伸长率达到最大值,其值分别为 12.3 N/mm 和 23.32%。同时,从模拟和 EBSD 结果可以看出,当初始厚度比为 20 时,层合板的变形协调能力最好,铝侧织构转变为剪切织构。当初始厚度比达到 40 后,层压板的结合性能降低,镁合金的性能占主导地位。

关键词: Al/Mg/Al 层合板; 大厚比; 力学性能; 界面结合强度; 显微组织

(Edited by Wei-ping CHEN)